Observational Cosmology Journal Club

July 1, 2013 Kento Masuda

1. Confirmation of hot Jupiter Kepler-41b via phase curve analysis

   E. V. Quintana et al., ApJ, 767, 137

2. Giant planets orbiting metal-rich stars show signatures of planet-planet interactions

   R. I. Dawson and R. A. Murray-Clay, ApJL, 767, L24

3. A simple, quantitative method to infer the minimum atmospheric height of small exoplanets

   D. M. Kipping, D. S. Spiegel & D. D. Sasselov, arXiv:1306.3221 (accepted in MNRAS)

1. Confirmation of hot Jupiter Kepler-41b via phase curve analysis

- A new method to confirm giant planets by
  - modeling the whole phase curve
  - eliminating all the possible false positives w/o the need for follow-up observations

common false positive (background eclipsing binary) →

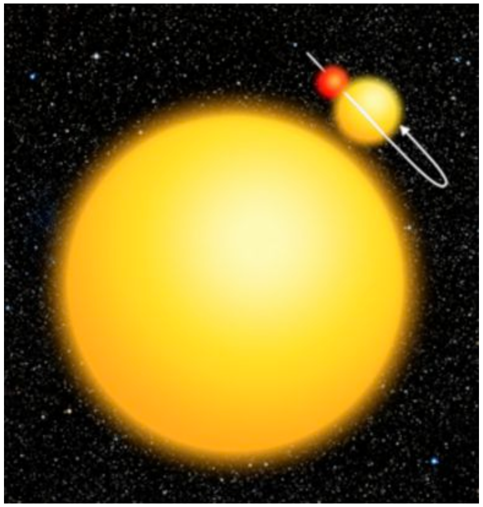

http://www.nasa.gov/mission_pages/kepler/multimedia/images/aas_conference.html

- Demonstration in Kepler-41system
  - Kepler-41(KOI-196): G6V star, K_p = 14.465
  - Kepler-41b: recently confirmed by RV

$$P = 1.86\mathrm{d},\ M_p = 0.55 \pm 0.09\ M_J$$

Phase curve modeling

- Transit → P, T_ϕ, R_p/R_*, b, ρ_*
- Occultation → ED (secondary eclipse depth)

+

- Ellipsoidal variation F_{ell} → A_{ell}

$$\frac{F_{\rm ell}}{F_{\rm tot}} = A_{\rm ell}\cos(2\pi\phi \times 2) \qquad A_{\rm ell} = \alpha_{\rm ell}\frac{M_{\rm p}}{M_*}\left(\frac{R_*}{a}\right)^3 \sin^2 i$$

- Doppler beaming F_{dop} → K (RV semi-amp.)

$$\frac{F_{\rm dop}}{F_{\rm tot}} = A_{\rm dop}\sin(2\pi\phi) \qquad A_{\rm dop} = \frac{-\alpha_{\rm dop}4K}{c}$$

- Reflected/emitted light F_{ref} → A_G

$$\frac{F_{\rm ref}}{F_{\rm tot}} = A_{\rm G}\left(\frac{R_{\rm p}}{a}\right)^2 \Psi(\phi)$$

Phase curve modeling

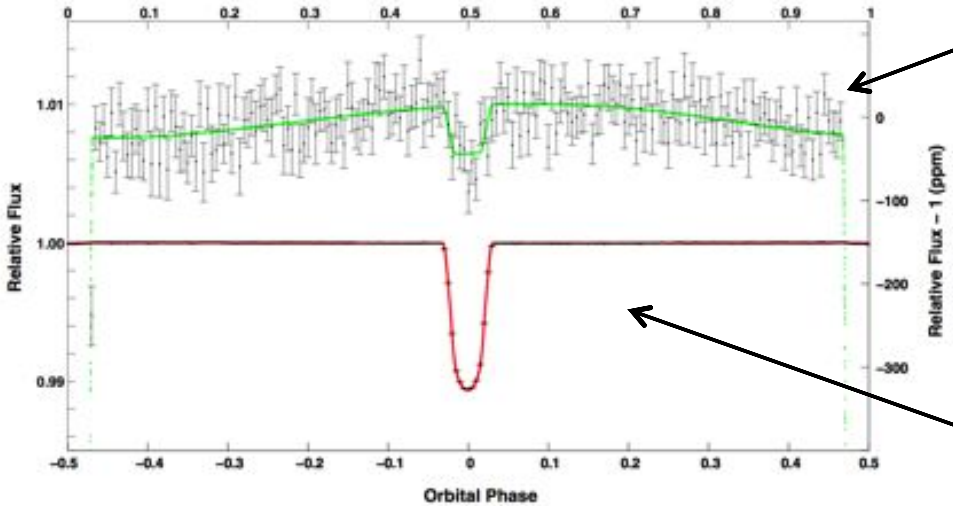

Figure 2. The detrended data for Kepler-41 phased to the orbital period and binned to 0.005 in phase. The red-lined data are centered on the transit and show the full phase and the green-lined data are centered on the occultation and magnified (see top and right axes). The green curve fits for ellipsoidal variations, Doppler boosting, and reflected/emitted light.

Centered on occultation (vertical scale magnified)

Centered on transit

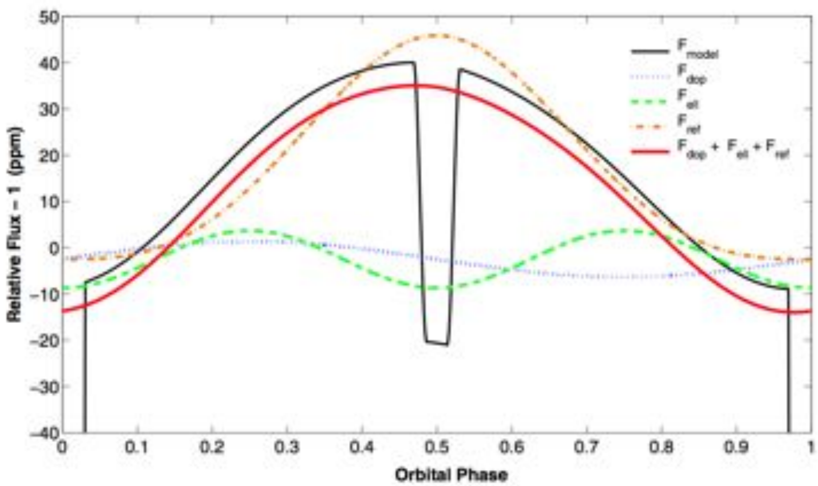

Figure 3. The best-fit model for Kepler-41b phased to the orbital period and magnified to show the occultation. Our full phase photometric model includes flux variations induced by the companion that can be decomposed. These include Doppler beaming (blue dotted curve), ellipsoidal variations (green dashed curve) and reflected/emitted light (orange dot-dashed curve). The sum of these three effects is shown in red. Note that we did not detect Doppler beaming in the light curve of Kepler-41, but we include a description of this effect in this article because it may be applicable to other planet candidates.

$M_p = 0.598^{+0.384}_{-0.598}\ M_J$

$R_p = 0.996^{+0.039}_{-0.040}\ R_J$

ED, A_{ell}, A_{ref} detected

Confirmation method

- Diluted models w/ dilution factor D = 1-100 %

 → Fit for the same parameters

 → Set limits on system parameters based on $\Delta\chi^2$

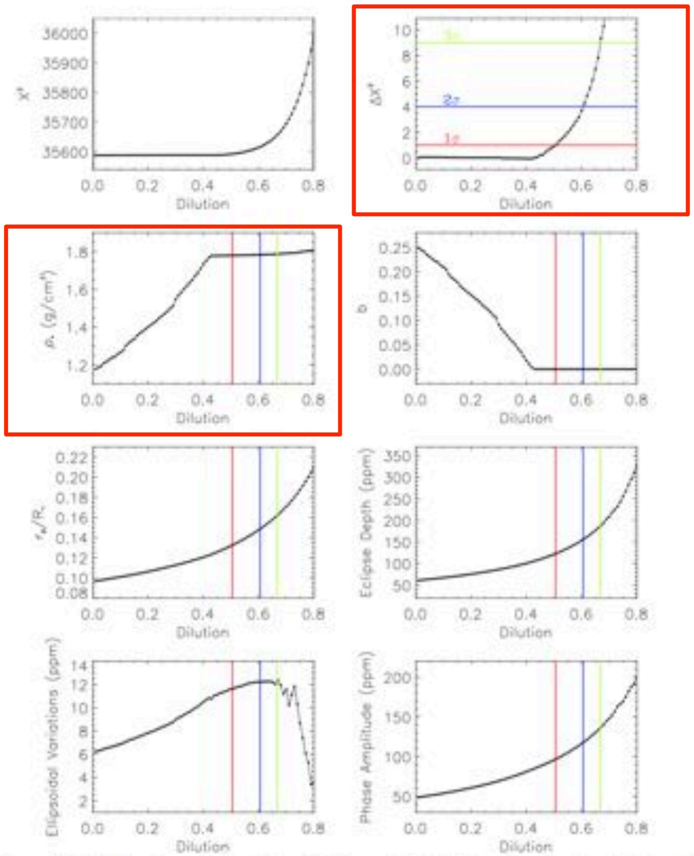

← $\Delta\chi^2$

D = 0.5(1σ), 0.6(2σ), 0.67(3σ)

ρ_* →

Figure 4. Results from our dilution model fits. The goodness-of-fit estimator χ^2 is shown in the top left panel as a function of dilution values that were injected into the light curve. We solve for the maximum allowed dilution (i.e., the maximum amount of third light from a potential blend) by measuring where $\Delta\chi^2$ changes by 1, 4, or 9 (corresponding to 1σ, 2σ, or 3σ), as shown in the top right panel by the red, blue and green horizontal lines, respectively. The lower six panels show six of the fit parameters as a function of dilution, and the red, blue, and green vertical lines determine their range of valid values as constrained by the dilution fits. Comparison of each valid dilution model to stellar evolution models rules out massive, stellar objects, confirming the planetary nature of Kepler-41b.

Confirmation method

- Stellar models (Yonsei-Yale)

→ (T_{eff}, R_*, ρ_*, log g) for full range of input (M_*, Z)

→ extract models w/ ρ_* within 3σ constraint + age < 14Gyr

→ (ρ_p, $T_{eff,p}$) for each model compared to the stellar models

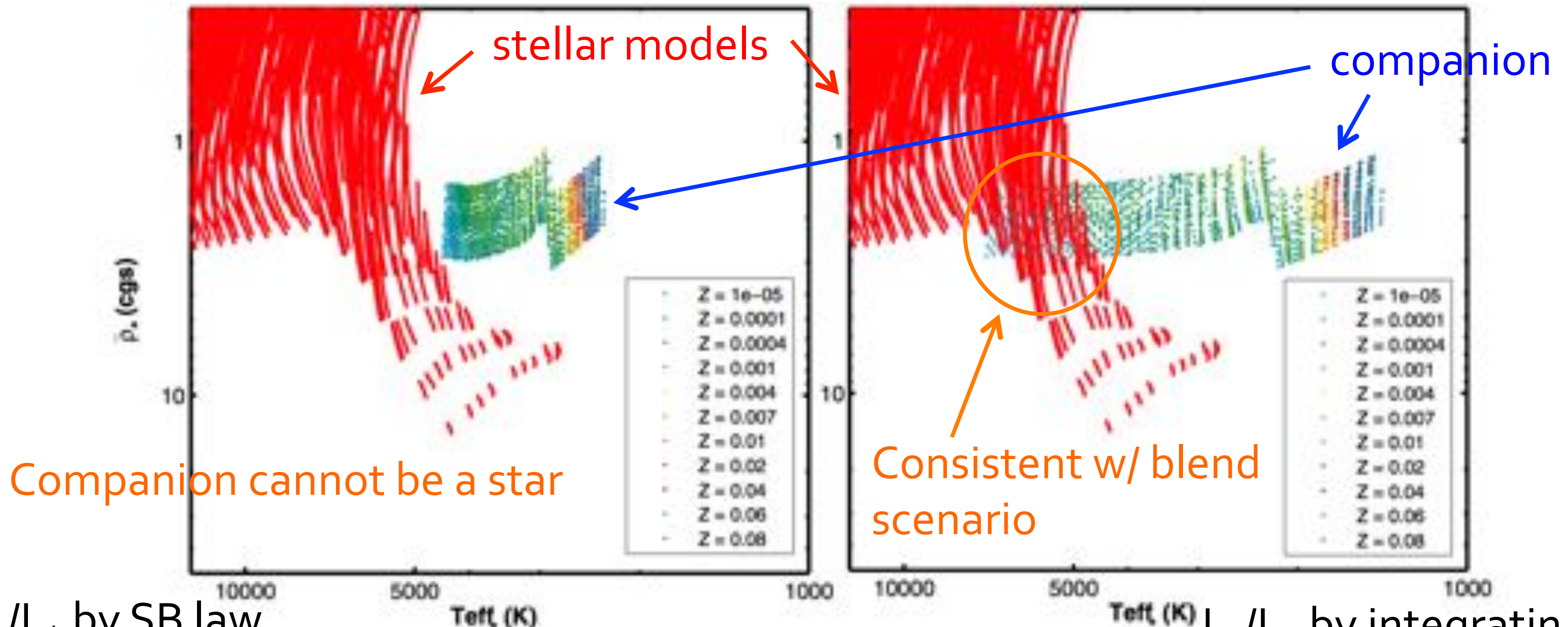

L_p/L_* by SB law

L_p/L_* by integrating Planck func.

Figure 5. The mean stellar density $\bar{\rho}_*$ is shown here as a function of T_{eff_*} for all available Yonsei-Yale stellar evolution tracks (shown by the red curves in each panel). The companion $\bar{\rho}_p$ and T_{eff_p} from the dilution model fits are overplotted for a range of metallicities Z (colored points in each panel). The dilution models in the left panel were computed using estimates of T_{eff_p} that were computed by integrating the planet and star Planck functions over the *Kepler* bandpass and comparing the ratio of the resulting luminosities to the secondary eclipse depth ED. All dilution models in this case are inconsistent with any stellar blend (there is no overlap with the stellar evolution tracks), and we can conclude that the companion to Kepler-41 is a planet. In the right panel, the dilution models were computed using T_{eff_p} values that were calculated from the ratio of the planet and star bolometric luminosities (over all wavelengths). This was done to determine if this simpler method (albeit not as precise) to compute T_{eff_p} is sufficient to rule out potential blends. In this case, a subset of dilution models overlap with stellar evolution tracks and therefore need to be examined further (see Figures 6 and 7) in order to rule out stellar blends.

Confirmation method

- Fig. 6: $T_{eq,p} \sim T_{eff,p} \rightarrow$ companion still consistent with planet
- Fig. 7: $M_p < 0.005 M_\odot$ in all the cases → cannot be a star !

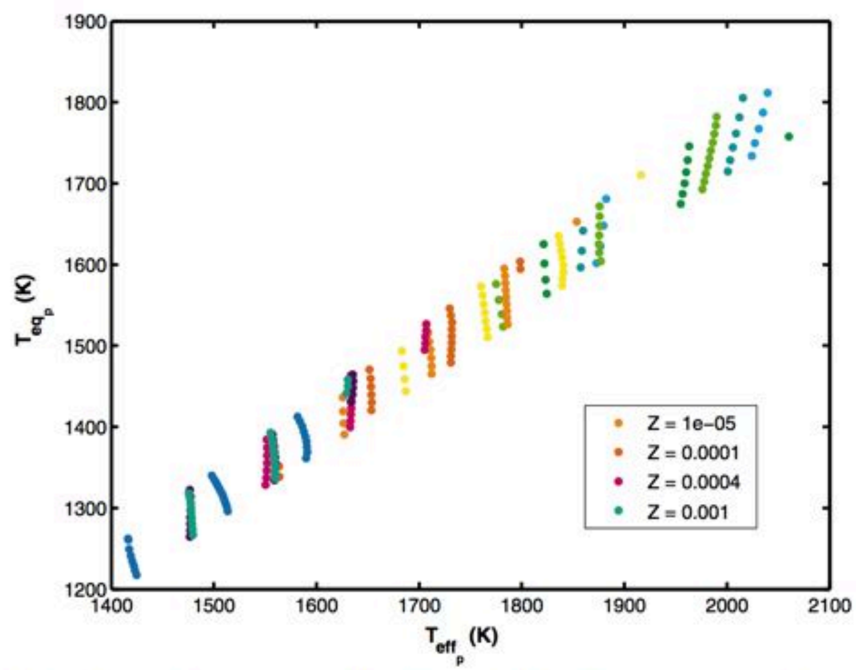

Figure 6. For the remaining valid dilution models (those that have parameters that overlap with stellar evolution tracks as shown in Figure 5), the equilibrium temperatures can be compared to the effective temperatures. To be of stellar nature, the values of $T_{\mathrm{eff_p}}$ for each model would need to be much greater than the corresponding values of $T_{\mathrm{eq_p}}$ (indicating that the companion is burning hydrogen). In this case, the temperatures are comparable and cannot be used to definitively rule out stellar blends, but this comparison may be useful to confirm other planet candidates.

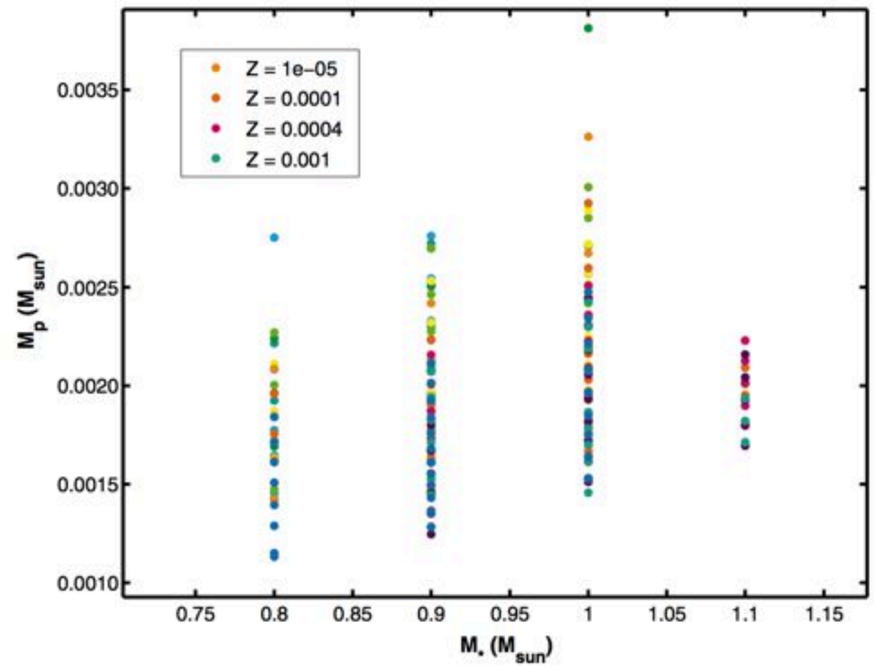

Figure 7. For the remaining valid dilution models (as shown in Figure 6), the relation between each companion mass M_p and the corresponding stellar mass M_* is shown here. All dilution models have a companion mass less than that needed for hydrogen burning ($\sim 0.08\, M_\odot$), indicating that the companion cannot be a star. With this comparison, we can eliminate these remaining dilution models and conclude that the companion to Kepler-41b is a planet.

2. Giant planets orbiting around metal-rich stars show signatures of planet-planet interactions

- “Valley” planets
  - a = 0.1-1 AU
  - also have migrated
  - outside the reach of tidal damping force

  → trends interpreted more easily

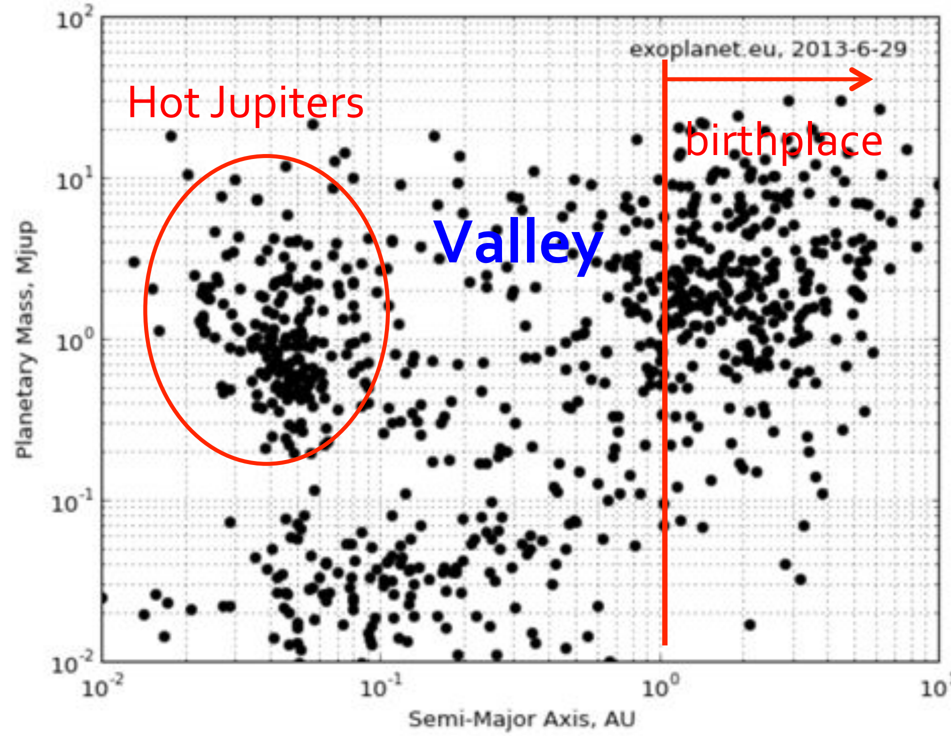

- Valley houses giants with a wide range of eccentricities

  → intermixing between two migration mechanisms

  → disk metallicity may determine which is triggered

Eccentricities of giant Valley planets

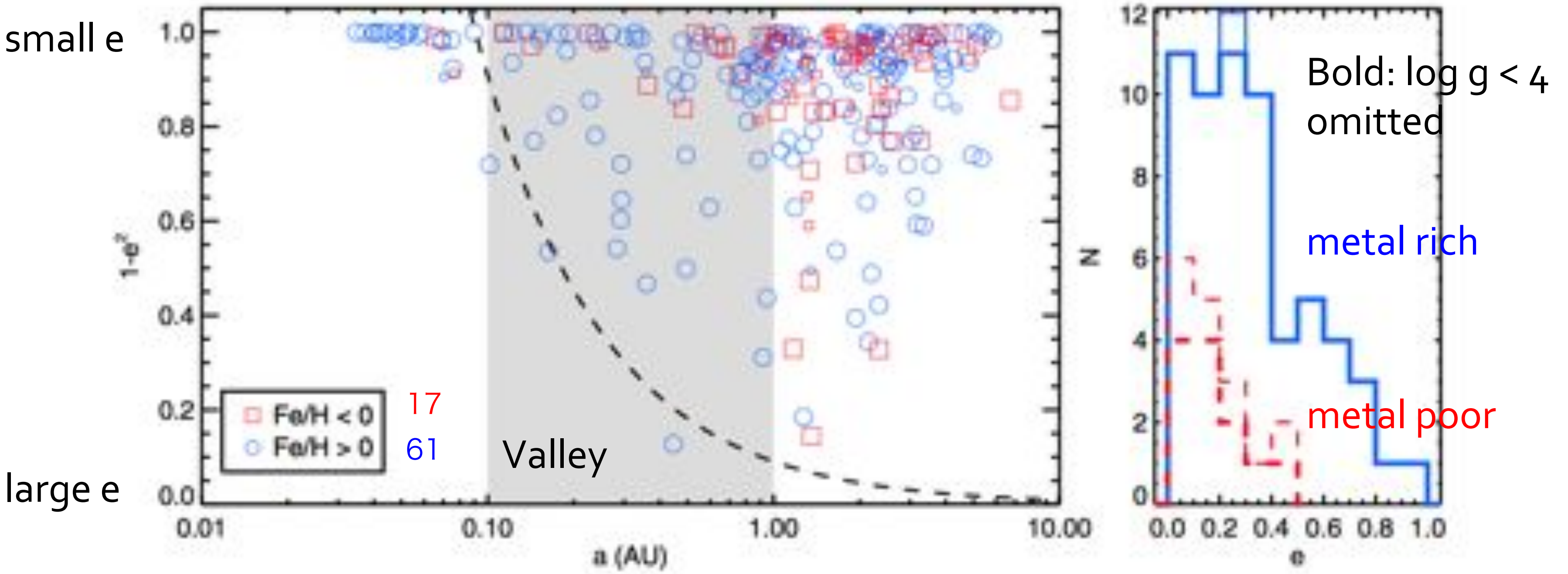

Figure 1. Left: Valley (gray region) giant planets orbiting metal-rich stars ([Fe/H] ⩾ 0; blue circles) have a range of eccentricities; those orbiting metal-poor stars ([Fe/H] < 0; red squares) are confined to low eccentricities. Small symbols represent stars with log g < 4. For reference, above the dashed line (a tidal circularization track ending at 0.1 AU) planets are unlikely to experience significant tidal circularization. We plot the quantity $1 - e^2$ to emphasize high-eccentricity planets. Right: eccentricity distributions of Valley planets orbiting metal-rich (blue solid) and metal-poor (red dashed) stars. The bold distributions omit stars with log g < 4.

- Only metal-rich stars host eccentric Valley planets ($e > 0.43$)
  → Closely packed multiple giants can only be formed around metal-rich stars ?

- Gas giants discovered by RV ($m \sin i < 0.1\ M_J$)
- FGK stars ($M_* = 0.4$ -1.4 $M_\odot$)

Eccentricities of giants under tidal circularization

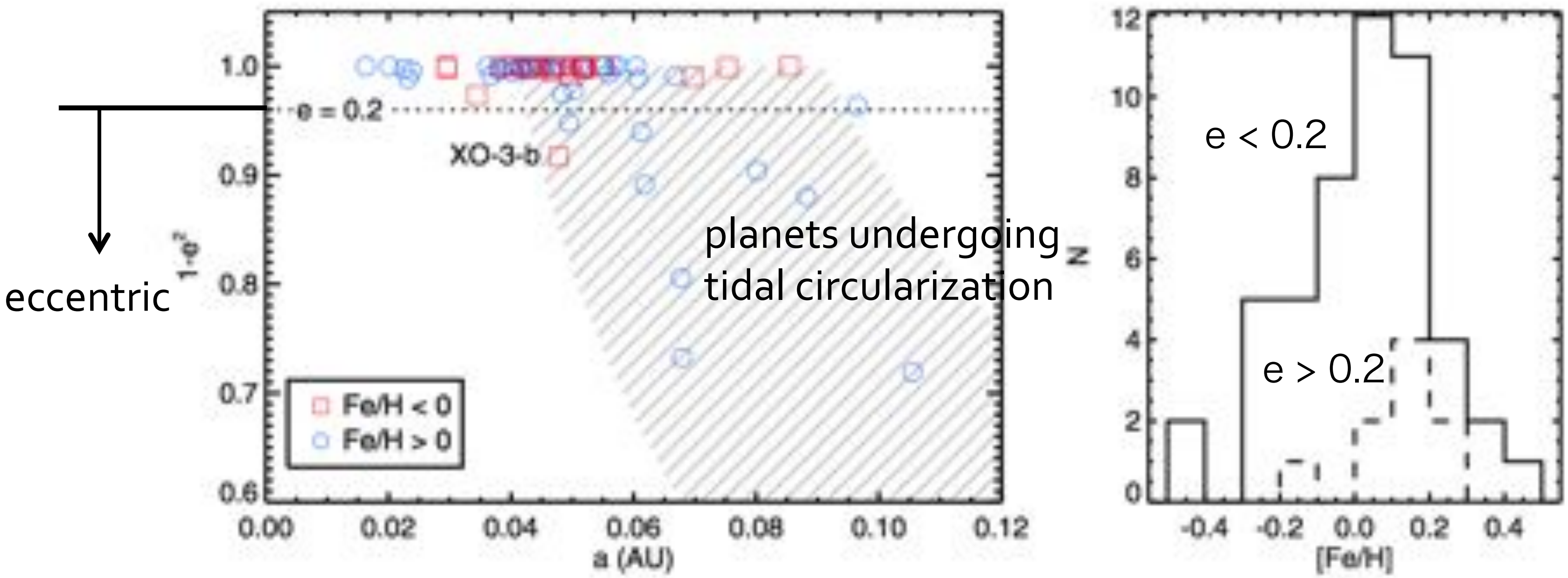

Figure 2. Left: giant planets discovered by non-*Kepler* transit surveys, orbiting metal-rich (blue circles) and metal-poor (red squares) stars. The striped region encloses planets undergoing tidal circularization to $3 < P_{\rm final} < 10$ days. Planets below the dotted line have $e > 0.2$, most of which orbit metal-rich stars. Right: distribution of host star metallicities for planets in the striped region (left) with $e > 0.2$ (dotted line) and $e < 0.2$ (solid line).

- Most observed eccentric planets orbit metal-rich stars

→ Only giant planets in metal-rich systems can be scattered onto eccentric orbits

- Giant planets detected by non-Kepler transit surveys
- FGK stars ($M_* = 0.4 - 1.4\ M_\odot$)

Giant planet period distribution

- $f_{HJ,Kepler}$ (Hot Jupiter occurrence rate in the Kepler sample) is smaller than $f_{HJ,RV}$ (in RV samples)
  ← due to systematically lower metallicities of Kepler host stars ?

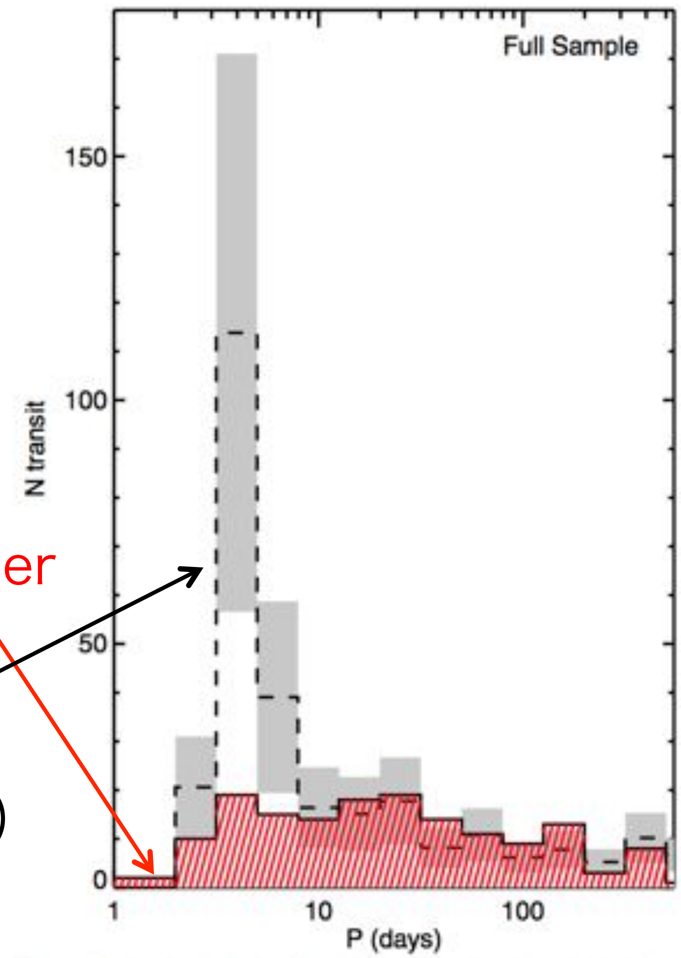

Figure 3. Red striped: number of transiting giant planets detected by *Kepler*. Black dashed: expected number based on the RV-discovered (i.e. excluding planets discovered by transit surveys) sample.[4] The gray error bars are from uncertainties in C_{norm}, not the Poisson uncertainties of each individual bin. The two distributions are consistent at long periods, but the *Kepler* sample lacks a short-period pile-up.

(A color version of this figure is available in the online journal.)

Period distribution of transiting giant planet candidates (R_p = 8 – 20 R_E) detected by Kepler

That expected from the RV sample
(taking account of different f_{HJ}, transit prob.)

- Kepler period distribution lacks a short period pile-up

Giant planet period distribution

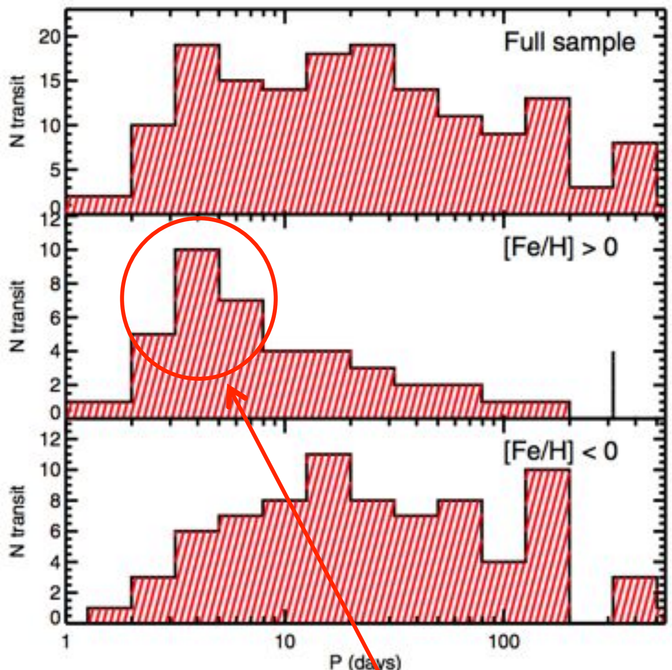

Figure 4. Number of transiting giant planets observed by *Kepler* without a stellar metallically cut (top), with [Fe/H] $\geqslant 0$ (middle), and with [Fe/H] < 0 (bottom). In the metal-rich sample (middle), we recover the shape of the short-period pile-up seen in the RV sample (black-dashed line, Figure 3). In contrast, the metal-poor sample (bottom) is depleted in short-period giants.

Kepler vs. RV for
metal-rich / metal-poor samples

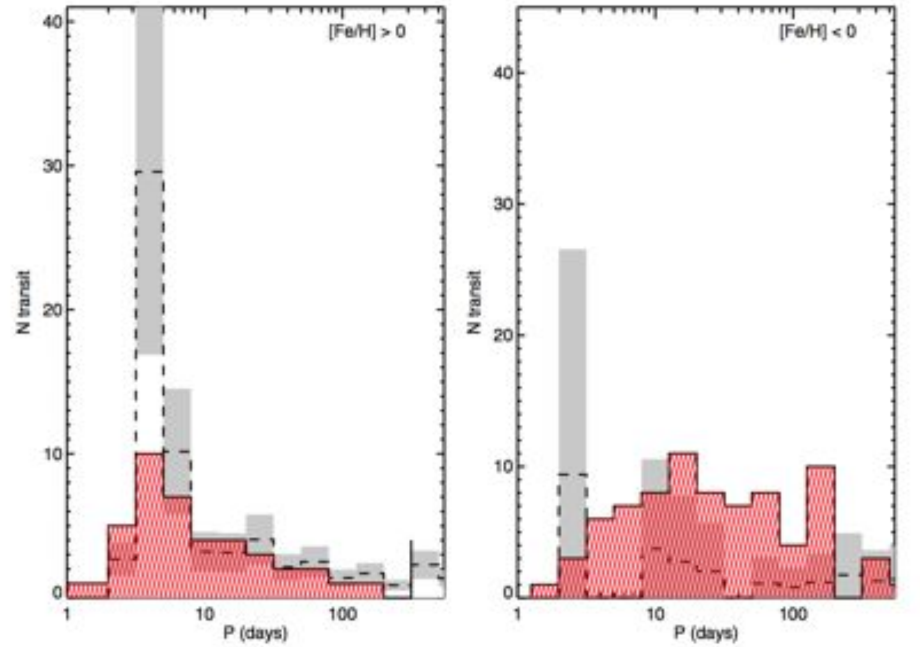

Figure 5. Same as Figure 3 but for metal-rich (left) and metal-poor (right) subsamples. Left: metal-rich *Kepler* sample (red striped) exhibits a short-period pile-up, but falls below RV expectations in the 3–5 day bin. Right: metal-poor *Kepler* sample is not inconsistent with the metal-poor RV sample, but the latter is difficult to characterize due to small numbers.

- Short-period pile-up is recovered in metal-rich samples

- Smaller discrepancy in metal-rich comparison (Fig. 5, left)
  → detailed follow-up motivated (precise estimated of f_{HJ})

Possible challenge for their interpretation

- Lack of the correlation between spin-orbit alignment and metallicity
  - not necessarily caused by dynamical perturbations ?
  - close-in planets are subject to tidal realignment

→ spin-orbit measurements of the Valley planets

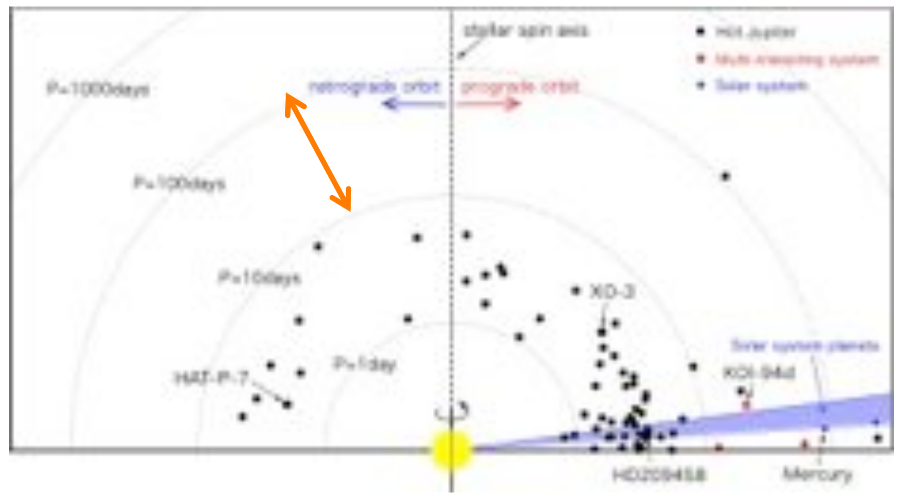

- Further tests
  - Assessments with a careful treatment of detection threshold
  - Theoretical assessments whether P-P scattering can also reproduce the Valley planets

3. A simple, quantitative method to infer the minimum atmospheric height of small exoplanets

- Mass-radius relation
  → two boundary conditions:
  1. maximum R_p - M_p contour
  2. minimum R_p - M_p contour for a pure-water planet

- Condition 2 can be violated if (and only if) a planet maintain an atmosphere

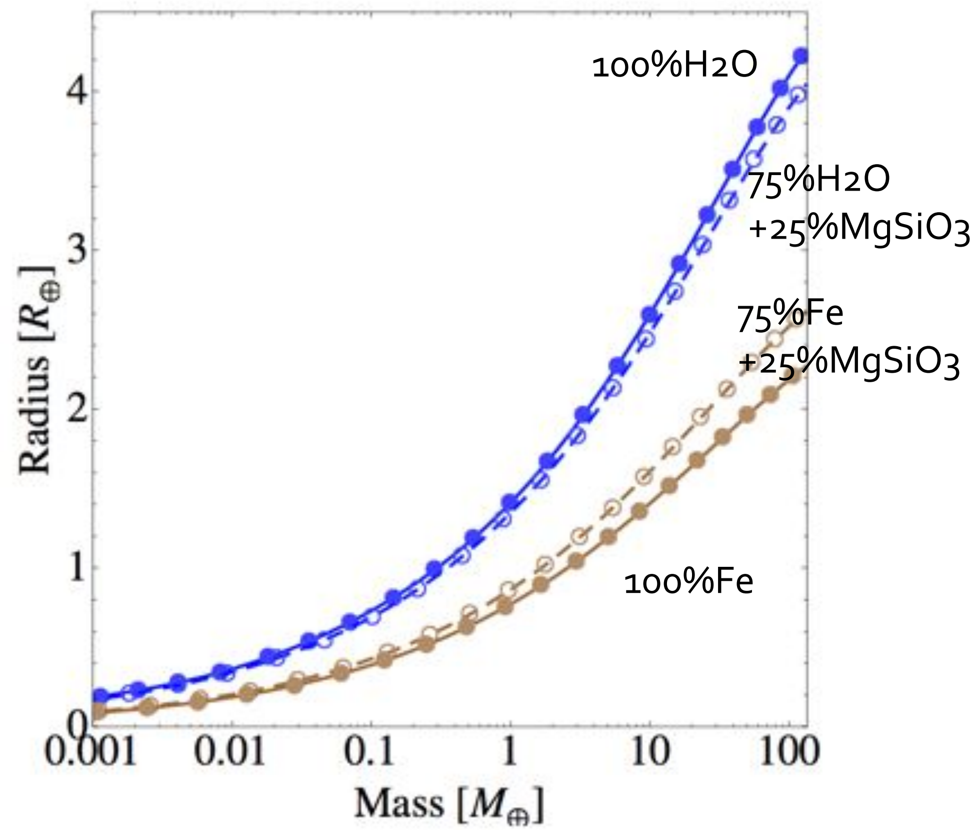

Figure 1. *Mass-radius diagram showing the range of plausible phases for an atmosphere-less Super-Earth (i.e. the boundary conditions), as derived from the model of Zeng & Sasselov (2013). Points taken from the model are shown as circles, along with our interpolation line shown overlaid. Blue is that of a 100%-H_2O planet, blue-dashed is 75%-H_2O-25%-$MgSiO_3$, brown is 100%-Fe and brown-dashed is 75%-Fe-25%-$MgSiO_3$.*

Method

- Minimum atmospheric height:

$$R_{\mathrm{MAH}}(R_P, M_P) = R_P - R_{P,\mathrm{H20}}(M_P)$$

Observed radius / mass of the planet 75%H_2O-25%$MgSiO_3$

- Confidence of the planet in question maintaining an atmosphere (i.e. $R_{MAH} > 0$):

$$\mathrm{P}(R_{\mathrm{MAH}} > 0) = \frac{\#\ \text{realizations where } R_{\mathrm{MAH}} > 0}{\#\ \text{realizations total}}$$

where R_p, M_p are drawn from the posterior joint probability distribution

Example

- GJ1214b
  - 2.8 R_E planet orbiting a nearby M4.5 dwarf
  - most well characterized small planet
  - R_{MAH} for 10^5 realizations

  → $P(R_{MAH} > 0) = 97.2\%$

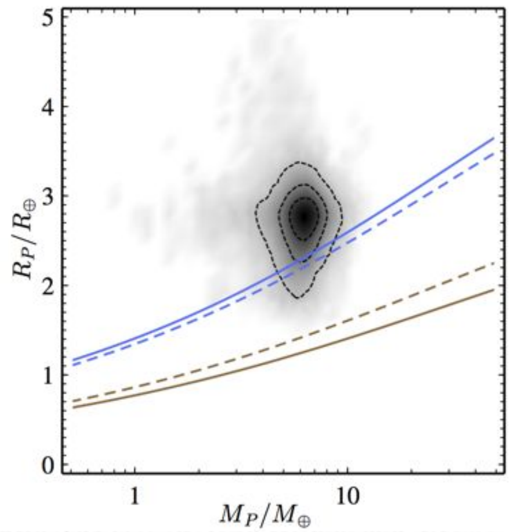

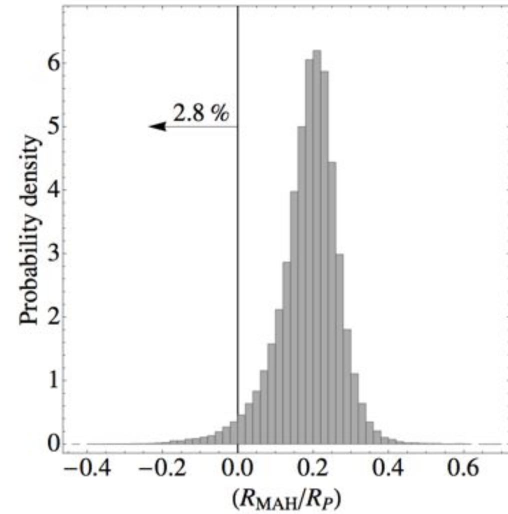

- Other examples

Table 3. *Example calculations of the minimum atmospheric height (MAH) for several planets. For Solar System planets quote the equatorial radius and assume sphericity, as is done for exoplanets.*

Planet	$M_P\,[M_\oplus]$	$R_P\,[R_\oplus]$	ρ_P [g cm^{-3}]	$R_{MAH}\,[R_\oplus]$	(R_{MAH}/R_P)	$P(R_{MAH} > 0)$ [%]
GJ-1214b	$6.19^{+0.80}_{-0.80}$	$2.75^{+0.18}_{-0.24}$	$1.66^{+0.56}_{-0.38}$	$+0.54^{+0.21}_{-0.24}$	$+0.197^{+0.061}_{-0.079}$	97.2
KOI-142b	$6.6^{+5.9}_{-6.1}$	$4.23^{+0.30}_{-0.39}$	$0.48^{+0.54}_{-0.45}$	$+2.07^{+1.00}_{-0.65}$	$+0.47^{+0.26}_{-0.12}$	> 99.9
Kepler-22b	$6.9^{+20.9}_{-6.2}$	$2.396^{+0.088}_{-0.181}$	$2.4^{+7.5}_{-2.2}$	$+0.11^{+1.04}_{-0.87}$	$+0.05^{+0.44}_{-0.37}$	54.5
Kepler-36b	$4.46^{+0.34}_{-0.27}$	$1.487^{+0.034}_{-0.035}$	$7.47^{+0.72}_{-0.59}$	$-0.537^{+0.042}_{-0.047}$	$-0.362^{+0.034}_{-0.038}$	< 0.01
Kepler-36c	$8.09^{+0.60}_{-0.45}$	$3.682^{+0.052}_{-0.056}$	$0.891^{+0.065}_{-0.045}$	$+1.327^{+0.049}_{-0.053}$	$+0.361^{+0.009}_{-0.012}$	> 99.99
Neptune	17.147	3.883	1.64	+1.08	+0.277	-
Uranus	14.536	4.007	1.27	+2.71	+0.325	-
Earth	1.000	1.000	5.52	-0.35	-0.350	-